Neural-Network-Based MPPT Control of a Stand-Alone Hybrid Power Generation System

Whei-Min Lin, *Member, IEEE*, Chih-Ming Hong, and Chiung-Hsing Chen

***Abstract*—A stand-alone hybrid power system is proposed in this paper. The system consists of solar power, wind power, diesel engine, and an intelligent power controller. MATLAB/Simulink was used to build the dynamic model and simulate the system. To achieve a fast and stable response for the real power control, the intelligent controller consists of a radial basis function network (RBFN) and an improved Elman neural network (ENN) for maximum power point tracking (MPPT). The pitch angle of wind turbine is controlled by the ENN, and the solar system uses RBFN, where the output signal is used to control the dc/dc boost converters to achieve the MPPT.**

***Index Terms*—Diesel engine, improved Elman neural network (ENN), maximum power point tracking (MPPT), photovoltaic (PV) power system, radial basis function network (RBFN), wind power system.**

I. Introduction

VARIABLE-SPEED wind turbines have many advantages that are well documented in the literature [1], [2]. The wind turbine can operate with maximum aerodynamic efficiency, and the power fluctuations can be absorbed as an inertial energy in the blades. In some applications, the wind turbine may be augmented by an additional power source, usually a diesel generator. These systems are called wind–diesel systems [3], [4] and may be used to supply electricity energy to stand-alone loads, e.g., small villages that are not connected to the main utility. Most diesel generation systems operate at a constant speed due to the restriction of constant frequency at the generator terminals. However, diesel engines have high fuel consumption when operating with light load and constant speed. In order to improve the efficiency and avoid wet stacking, a minimum load of about 30% to 40% is usually recommended by the manufacturers [5]. Variable-speed operation can increase the efficiency, where the fuel consumption can be reduced up to 40% [5], especially when operating with a light load. Moreover, the life expectancy can increase with a lower thermal signature. To avoid the frequent start/stop of the diesel generator, an energy storage system is often used.

Topologies of the power electronic converter for maximum power point tracking (MPPT) [6] and voltage conversion are studied in this paper. The maximum power point of photovoltaic (PV) array is variational, so a search algorithm is needed according to the current–voltage (I–V) and power–voltage (P–V) characteristics of the solar cell. The perturbation and observation (P&O) MPPT algorithm is commonly used, due to its ease of implementation. It is based on the observation that if the operating voltage of the PV array is perturbed in a given direction and the power drawn from the PV array increases, which means that the operating point is moving toward the MPP, so the operating voltage must be further perturbed in the same direction. Otherwise, with the operating point moving away from the MPP, the direction of the operating voltage perturbation must be reversed. By using the P&O method, impedance matching is conducted between a boost converter and PV array in order to realize the MPPT function [7], [8].

Diesel generators are normally used to supply power to remote areas where grid connection is not available. However, power generation from diesel generators is not environmental friendly as they produce pollutant gases and the price of the diesel is on the rise. Considering the environmental and economic aspect of a diesel generator, it is better to generate power from a cost-effective, environmental friendly renewable energy, such as wind, solar, and hydro. There are some works on hybrid systems [9], where the dynamic performance of a stand-alone wind-solar system with battery storage was analyzed. Methodologies for optimal design or unit sizing of stand-alone or grid-connected hybrid systems were proposed using steady-state analysis [10]–[12], where the steady-state performance of a grid-connected wind-PV system with battery storage was also analyzed [13].

The general requirements of MPPT are: simple, low cost, quick tracking when condition changes, and small output power fluctuation. The traditional methods are simple and low cost without good tracking performance, such as hill climbing, P&O, and incremental conductance, etc. Novel methods are developed with higher accuracy but complex process, such as the optimum gradient method, fuzzy logic control, and neural networks (NN). These technique could also be costly, difficult to implement, and may not be stable enough [7], [8]. Radial basis function network (RBFN) has a faster convergence property than common multiplayer-perceptron NN, but with a simpler network structure. RBFN also has a similar feature as the fuzzy-logic system, where the output value is calculated using the weighted-sum method, and the number of nodes in the hidden layer is the same

Manuscript received January 9, 2011; revised March 11, 2011, May 9, 2011, and June 27, 2011; accepted July 2, 2011. Date of current version December 6, 2011. This work was supported by the National Science Council in Taiwan, R.O.C., through its grant NSC 100-3113-P-110-003 and NSC 100-3113-E-194-001. Recommended for publication by Associate Editor M. Molinas.

W.-M. Lin and C.-M. Hong are with the Department of Electrical Engineering, National Sun Yat-Sen University, Kaohsiung 80424, Taiwan, R.O.C. (e-mail: wmlin@mail.ee.nsysu.edu.tw; d943010014@student.nsysu.edu.tw).

C.-H. Chen is with the Department of Electronic Communication Engineering, National Kaohsiung Marine University, Kaohsiung 81157, Taiwan, R.O.C. (e-mail: chiung@mail.nkmu.edu.tw).

Color versions of one or more of the figures in this paper are available online at http://ieeexplore.ieee.org.

Digital Object Identifier 10.1109/TPEL.2011.2161775

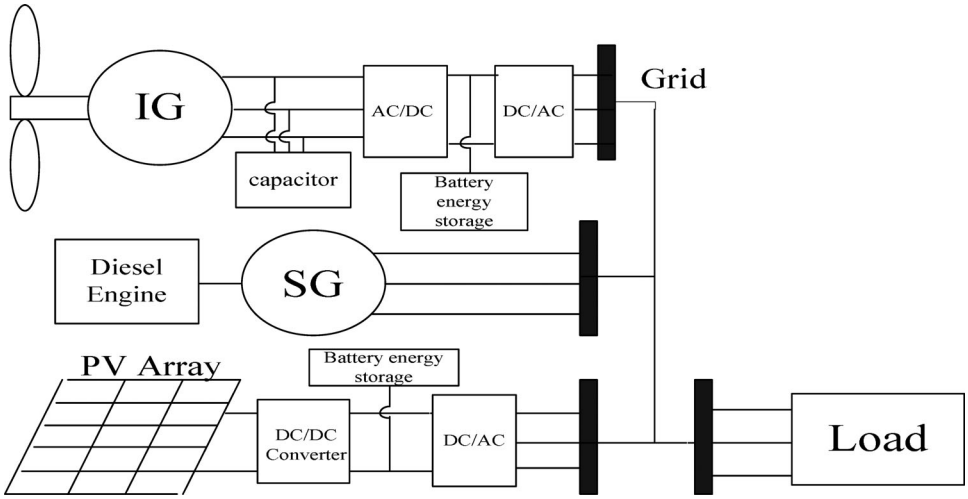

Fig. 1. Proposed hybrid system.

as that of the "if–then" rules of the fuzzy system. The receptive field functions of the RBFN are also similar to the membership functions of the premise part of the fuzzy-logic system. With advantages of multiple facets and the self-adapting capabilities, RBFN is very useful for controlling nonlinear and time-varying dynamic systems where uncertainties and parameter variations need extra attention [14].

Li *et al*. [15] proposed a small wind generation system with NN for wind-speed estimation and PI control for maximum wind-power extraction. The mechanical power of the wind turbine can be well tracked for both the dynamic and steady state, but the power deviation and speed tracking errors are large for transient response lasting for almost 20 s. Muljadi and Butterfield developed pitch control and generator load control methods to adjust the aerodynamic power, but power coefficient C_p deviation is too large [16]. The Elman neural network (ENN) is a partial recurrent network model first proposed by Elman [17], where the dynamic characteristics are provided by internal connections. The ENN does not need to use the state as input or training signal, which makes the ENN superior to static feedforward network and is used in dynamic system identifications widely [18]. In order to improve the ability of identifying high-order systems, some modified ENN have been proposed recently, which proved to have more advantages than the basic ENN, including a better performance, higher accuracy, dynamic robustness, and a fast transient performance.

Nowadays, the growth of wind and PV power generation systems has exceeded the most optimistic estimation [18]–[20]. In this paper, a stand-alone hybrid energy system consisting of wind, PV and diesel is proposed with the battery for energy storage. Wind and PV are the primary power sources of the system to take full advantages of renewable energy, and the diesel is used as a backup system. The dynamic modeling and control of the system is studied. The concept and principle of the hybrid system with its supervisory control were delineated. Classical techniques of maximum power tracking were applied to PV array and the wind-turbine control.

II. System Overview and Model Description

The proposed solar and diesel–wind hybrid system is shown in Fig. 1. Dynamic models of the main components were developed using MATLAB/Simulink, consisting of

1) wind energy conversion system (WECS);
2) diesel generator system;
3) PV generation system;
4) battery energy storage system (BESS).

A. Wind Energy Conversion System

In order to capture the maximal wind energy, it is necessary to install the power electronic devices between the wind turbine generator (WTG) and the grid where the frequency is constant. The input of a wind turbine is the wind and the output is the mechanical power turning the generator rotor [6]. For a variable-speed wind turbine, the output mechanical power available from a wind turbine could be expressed as

$$P_m = \frac{1}{2}\rho A C_p(\lambda, \beta) V_\omega^3 \tag{1}$$

where ρ and A are the air density and the area swept by blades, respectively. V_ω is the wind velocity (m/s), and C_p is called the power coefficient, and is given as a nonlinear function of the tip speed ratio λ defined by

$$\lambda = \frac{\omega_r r}{V_\omega} \tag{2}$$

where r is the wind turbine blade radius, and ω_r is the turbine speed. C_p is a function of λ and the blade pitch angle β.

A variable-speed pitch-regulated wind turbine is considered in this paper, where the pitch angle controller plays an important role. Fig. 2 shows the groups of C_p–λ curves of the wind turbine used in this study at different pitch angles [10]. It is noted from the figure that C_p can be changed by adjusting the pitch angle β. In other words, the output power of the wind turbine can be regulated by pitch angle control.

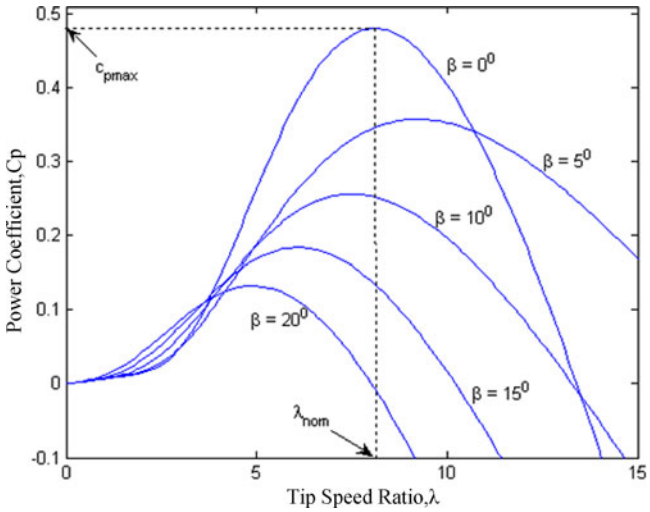

Fig. 2. C_p–λ characteristics of the WECS at different pitch angles.

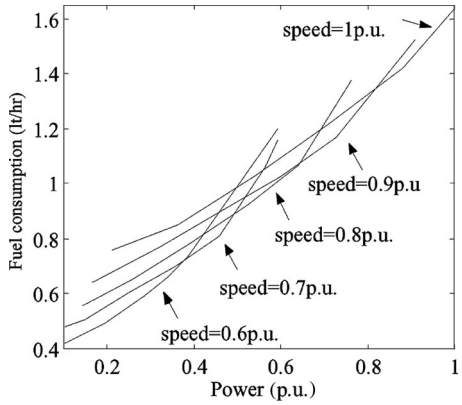

Fig. 3. Fuel consumption versus power at various rotational speeds.

B. Diesel-Generator Set Model

The diesel-generator set (DGS) model is composed of combustion, drive train, and synchronous generator models. A common governor model is used in this paper; the essential features can be described by the transfer function described in [3].

The fuel consumption of a diesel engine depends on the speed and torque of the machine. Fig. 3 shows the fuel consumption curves of a diesel engine for various rotational speeds. It can be seen that at 20% rated power, there is a 50% fuel saving than that at 0.6 rated speed. According to Fig. 3, a continuous function for the optimal operation versus speeds can be formed tangent to all the curves. In order to minimize the fuel consumption, the speed demand (optimum speed) for the diesel engine is calculated by building up a look-up table where the optimal power-speed curve is implemented.

C. Excitation System

The excitation system used in diesel generator is Type-1 excitation model taken from IEEE Standard 421.5 [21].

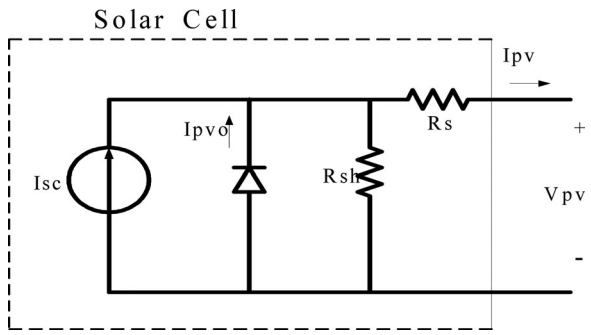

Fig. 4. Equivalent circuit of a solar cell.

D. Photovoltaic Array Model

Solar cell is a p-n junction, with characteristics similar to diodes. Parameters of the solar cell are shown in Fig. 4.

The relation between the array terminal current and voltage is [7]

$$V_{\rm PV} = \frac{nKT}{q} \ln\left(\frac{I_{\rm SC}}{I_{\rm PV}} + 1\right) \tag{3}$$

$$I_{\rm PV} = I_{\rm SC} - I_{\rm PVO}\left[\exp\left(\frac{q\left(V_{\rm PV} + I_{\rm PV}R_S\right)}{nKT}\right) - 1\right] - \frac{V_{\rm PV} + R_S I_{\rm SC}}{R_{\rm sh}} \tag{4}$$

where R_s and $R_{\rm sh}$ are series and shunt resistances, respectively. $I_{\rm SC}$ is the light induced current, n is the ideality factor of p-n junction, $I_{\rm PVO}$ is the diode saturation current, K is Boltzmann constant (8.63×10^{-5}J/°K), and q is the electronic charge. $I_{\rm SC}$ depends on the irradiance level S and the array temperature T with

$$I_{\rm SC} = I_{\rm ref}\left[1 + ht(T_c - T_{\rm ref})\right]\frac{S}{S_{\rm ref}} \tag{5}$$

where $I_{\rm ref}$ is the short-circuit current under the reference irradiance strength $S_{\rm ref}$ and temperature $T_{\rm ref}$, ht is cell module temperature coefficient, while $I_{\rm PVO}$ depend on T only [7], [22].

E. Output Characteristics of Solar Cell

The output characteristics are drastically affected by the irradiation and temperature. Equations (3)–(4) show that the solar cell has nonlinear output characteristics. The *P–V* and *I–V* characteristics are shown in Fig. 5. When the output voltage change of solar array is small, the change of output current is extremely small and the solar array is considered as a constant current source. However, the current decreases quickly as the voltage exceeds a critical value.

F. Battery Energy Storage System

The battery load current rapidly changes according to changes in weather conditions and power command for the bus inverter in operation. The dc-bus voltage must be regulated to stay within a stable region regardless of the battery-current variation. When the dc bus voltage $V_{\rm dc}$ becomes larger than the upper limit $V_{\rm dc\_up}$, charging mode begins with the voltage command $V_{\rm dc}^*$

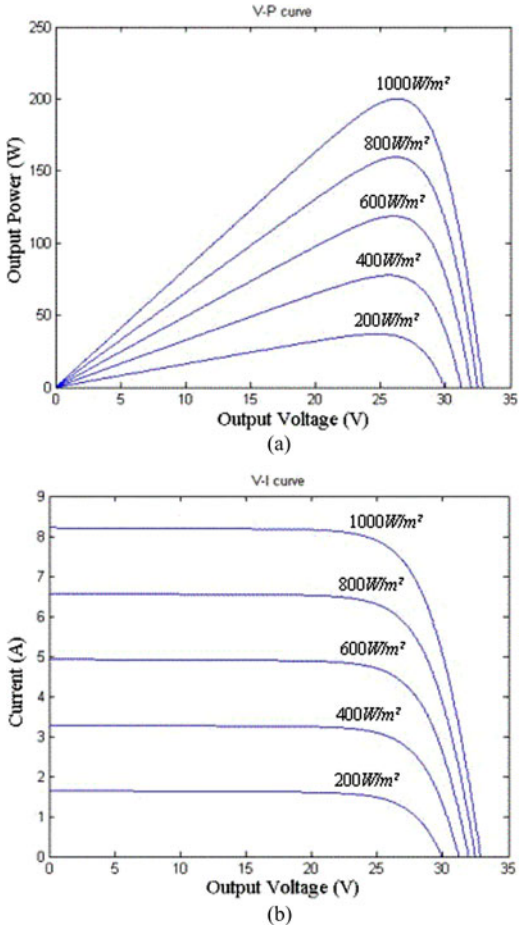

Fig. 5. *P–V* and *I–V* characteristics of solar cell.

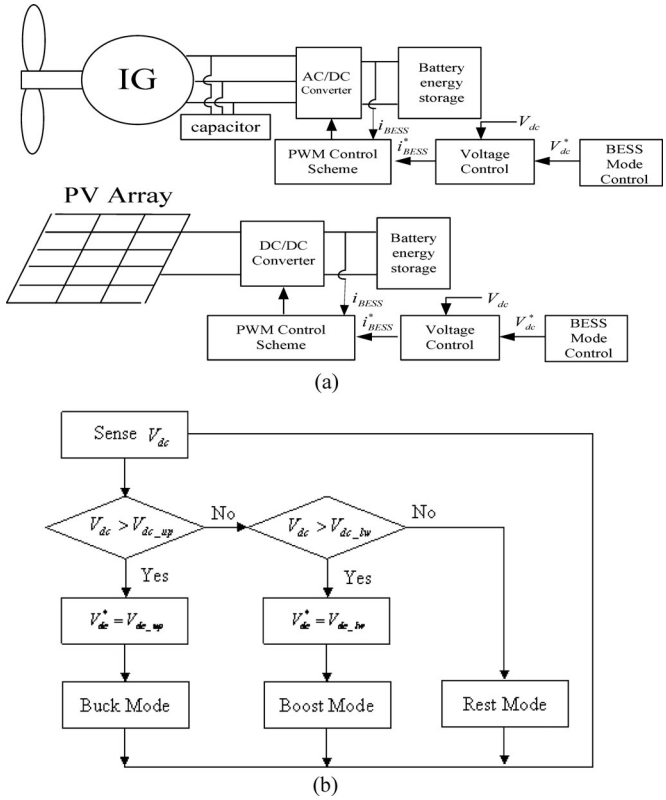

Fig. 6. Configuration of BESS control schematic. (a) BESS structure and interconnection diagram. (b) battery-mode control block.

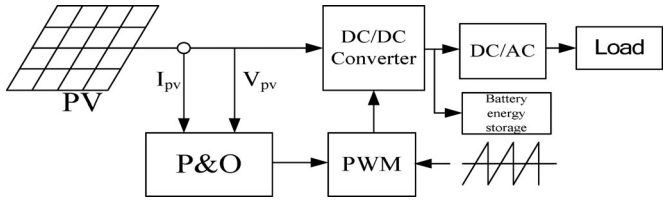

Fig. 7. Configuration of the P&O control system.

equal to the upper limit and continues until the dc voltage reaches the limit. If $V_{\rm dc}$ goes below the lower limit $V_{\rm dc\_lw}$, then the voltage target is bounded at the lower limit and the converter starts operating in boost mode. Accordingly, the battery-mode control block in Fig. 6(a) can be built as shown in Fig. 6(b).

III. MPPT Control Algorithm of the PV System

With the cost of solar cell, it is necessary to implement MPPT to have the voltage operating close to the maximum power point under the changing environment. The proposed PV system is composed of an array of 4 × 4 panels, a dc/dc converter, battery storage, a dc/ac inverter, and a control algorithm, generally performed by a microcontroller to track the maximum power continuously. MPPT is also used to provide a constant voltage to the required load.

A. P&O Method

The most common method in this field is the P&O method [12]. It periodically increases or decreases the solar cell's voltage as mentioned before to seek the maximum power point. In this paper, a variable step method is proposed to search for the maximum power point, where the step length is adjusted according to the distances to the MPP. The ratio of the variation of power P to voltage V is considered as the step length of duty ratio D, which is actually the slope of each operating point under very short sampling time. Fig. 7 shows the control block of the P&O method.

B. RBFN Controller Design

A three-layer RBFN NN with a boost converter shown in Fig. 8 is adopted to implement the controller [23], [24] where the control law $V_{\rm MPPT}$ is generated, and $x_1^1 = V_{\rm PV}$, $x_2^1 = I_{\rm PV}$, and $x_3^1 =$ Temperature. In the proposed RBFN, the number of units in the input, hidden, and output layers are three, nine, and one, respectively. In order to apply RBFN control, PV system in Fig. 9 is linearized in this section. The PWM module is used to generate PWM pulses to control the duty cycle of the switch.

1) Basic Nodes Operation: Layer 1: Input Layer

The nodes in this layer are used to directly transmit the numerical inputs to the next layer. The net input and output are

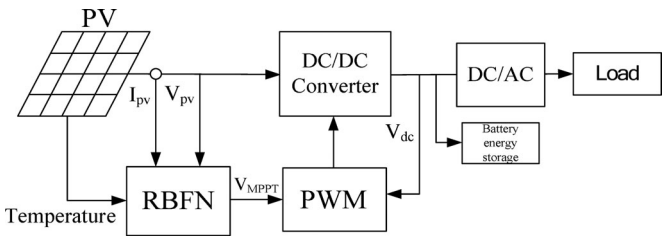

Fig. 8. Configuration of the RBFN control system.

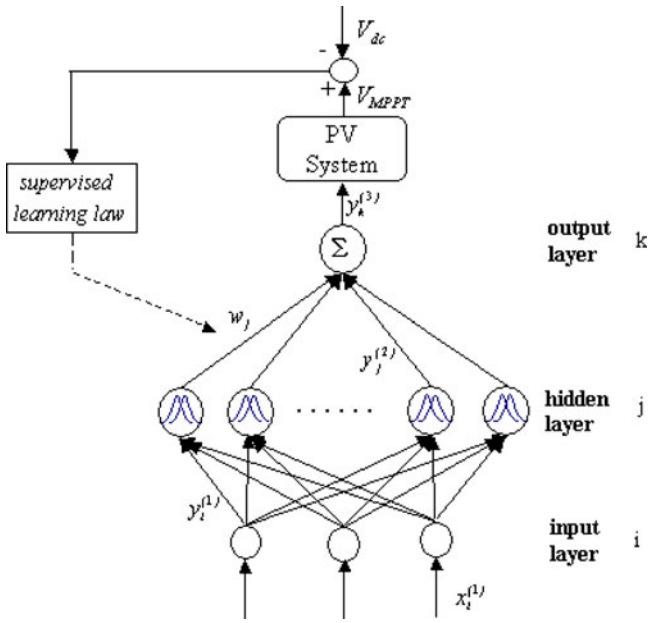

Fig. 9. Structure of the three-layer RBFN.

represented as

$$\text{net}_i^{(1)} = x_i^{(1)}(N) \tag{6}$$

$$y_i^{(1)}(N) = f_i^{(1)}\left(\text{net}_i^{(1)}(N)\right) = \text{net}_i^{(1)}(N), \quad i=1,2 \tag{7}$$

Layer 2: Hidden Layer

Every node performs a Gaussian function. The Gaussian function, a particular example of radial basic functions, is used here as a membership function. Then

$$\text{net}_j^{(2)}(N) = -(X - M_j)^T \sum_j (X - M_j) \tag{8}$$

$$y_j^{(2)}(N) = f_j^{(2)}\left(\text{net}_j^{(2)}(N)\right) = \exp\left(\text{net}_j^{(2)}(N)\right), \quad j = 1, \ldots, 9 \tag{9}$$

where $M_j = [\, m_{1j} \quad m_{2j} \quad \cdots \quad m_{ij} \,]^T$ and $\sum_j = \text{diag}\,[\, 1/\sigma_{1j}^2 \quad 1/\sigma_{2j}^2 \quad \cdots \quad 1/\sigma_{ij}^2 \,]^T$ denote the mean and the standard deviation of the Gaussian function.

Layer 3: Output Layer

The single node *k* in this layer is denoted by Σ, which computes the overall output as the summation of all incoming signals by

$$\text{net}_k^{(3)} = \sum_j w_j y_j^{(2)}(N) \tag{10}$$

$$y_k^{(3)}(N) = f_k^{(3)}(\text{net}_k^{(3)}(N) = \text{net}_k^{(3)}(N) \tag{11}$$

where w_j is the connective weight between the hidden and the output layers.

2) Supervised Learning and Training Process: Once the RBFN has been initialized, a supervised learning law of gradient descent is used to train this system. The derivation is the same as that of the back-propagation algorithm. It is employed to adjust the parameters m_{ij}, σ_{ij}, and w_j of the RBFN by using the training patterns. By recursive application of the chain rule, the error term for each layer is calculated, and updated. The adjustment of the parameters for learning and the weight of links enhance the performance of solar systems. The purpose of supervised learning is to minimize the error function *E* expressed as

$$E = \frac{1}{2}\left(V_{\text{dc}} - V_{\text{MPPT}}\right)^2 \tag{12}$$

where V_{dc} and V_{MPPT} represent the reference output voltage and the actual output voltage. A common supervised training algorithm is used in this paper, the essential features can be found in [23] and [24].

IV. MPPT Control Algorithm of the Wind Energy System

A. Wind Energy Controller Design

The wind power generation system studied in this paper is shown in Fig. 10, composed of an induction generator, a current control PWM ac/dc converter, a field-orientation mechanism including the coordinate translator, a current controlled dc/ac inverter, and the MPPT controller, where the PI and ENN were studied in this paper. The dc-bus voltage is regulated at a constant value so the real power from the wind turbine can pass to the grid. By using the reference frame theory and the linearization technique, the field-oriented induction generator system can be reasonably represented by the control system block diagram shown in Fig. 11.

B. Design of the PI Controller

The PI controller is used in Fig. 11(a). The desired step command tracking response for high performance applications usually are: 1) no steady-state error; and 2) preset rising time. In addition to these two criteria, this research will further suppress the overshoot. Using the nominal plant model, the transfer function of the power response to the command input in Fig. 11(a) can be expressed by

$$\left.\frac{P_{\text{out}}(s)}{P_{\text{ref}}(s)}\right|_{T_m(s)=0} = \frac{K_I K_t}{Js^2 + (B + K_p K_t)s + K_I K_t} \triangleq \frac{\omega_n^2}{s^2 + 2\zeta\omega_n s + \omega_n^2} \tag{13}$$

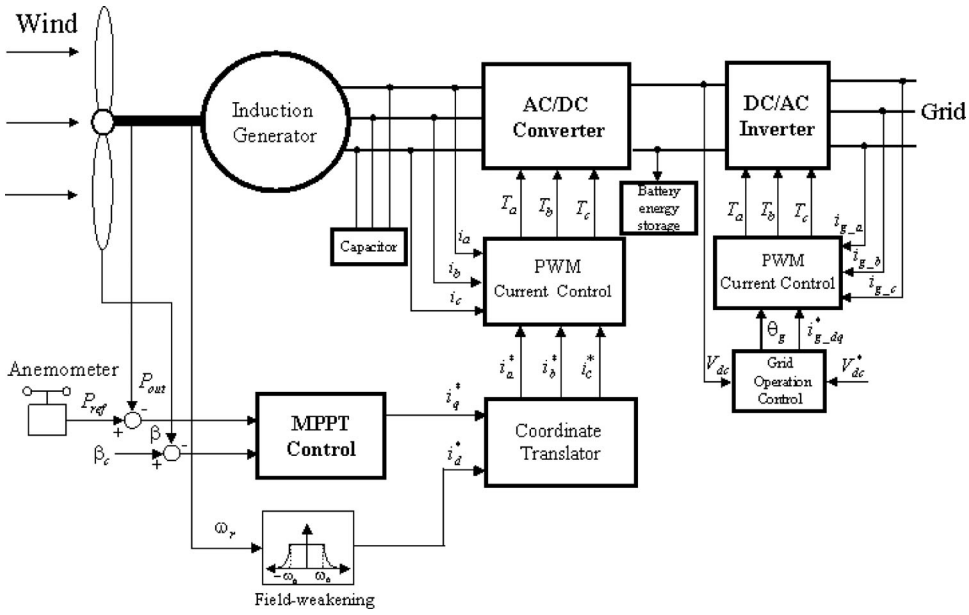

Fig. 10. Configuration of the wind-generation system.

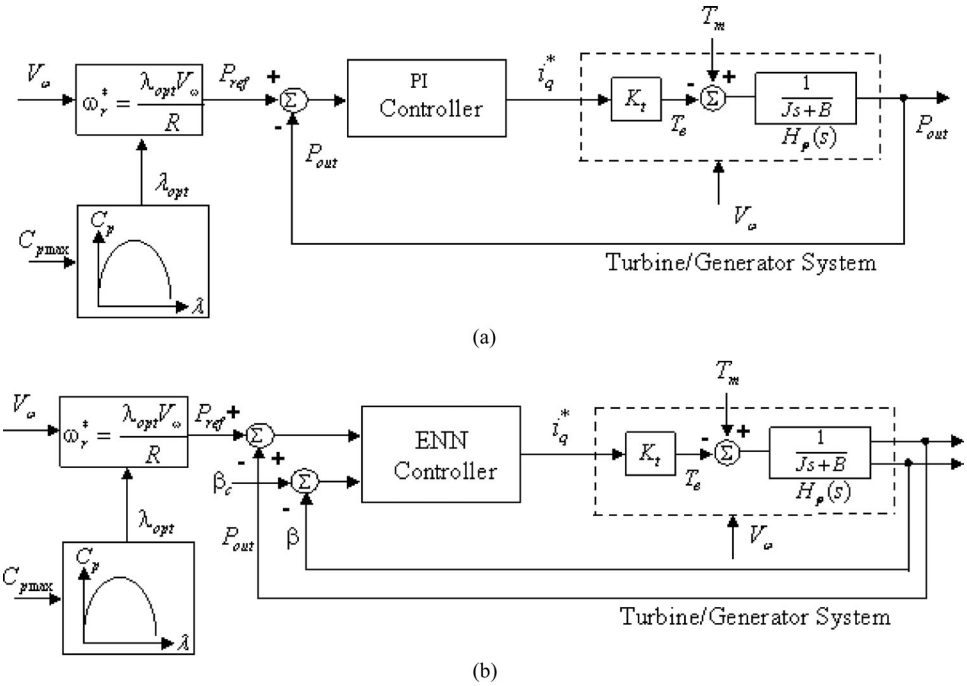

Fig. 11. Wind energy control system. (a) PI controller. (b) ENN controller.

where

$$\zeta = \frac{B + K_p K_t}{2(JK_I K_t)^{1/2}}, \quad \omega_n = \left(\frac{K_I K_t}{J}\right)^{1/2}. \tag{14}$$

computed using

$$K_I = \frac{J\omega_n^2}{K_t}, \quad K_p = \frac{(2J\omega_n - B)}{K_t}. \tag{15}$$

With the absence of zeros, the overshoot of the step response in (13) can be avoided by setting the damping ratio $\zeta = 1$. If the unknown parameter ω_n is solved according to the prescribed specifications, the parameters of the PI controller can be

Equation (13) also indicates that the tracking steady-state error is zero. It follows from the previous analysis that the desired tracking specifications can be completely achieved by using the simple PI controller.

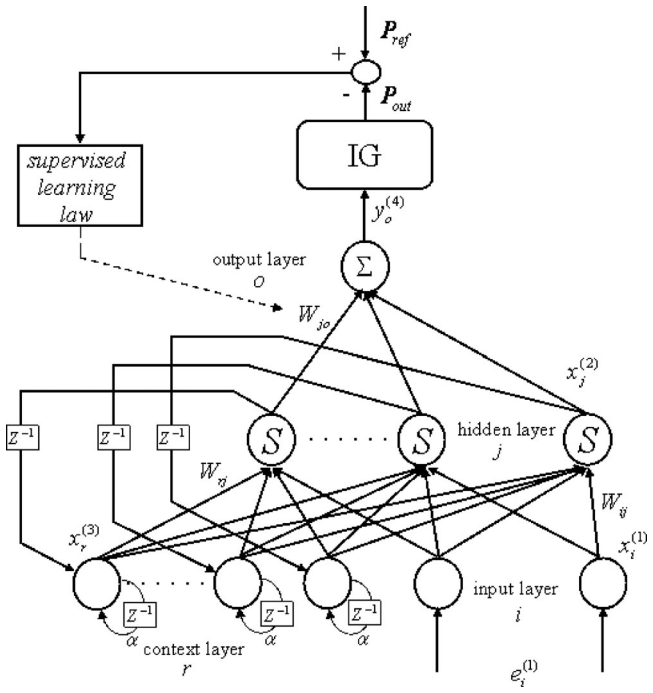

Fig. 12. Architecture of the ENN.

C. Improved ENN Controller Design

The architecture of the proposed ENN including the input layer, the hidden layer, the context layer, and output layer with two inputs and one output is shown in Fig. 12, where the control law is defined as i_q^*, and the ENN input is $e_1^{(1)}$ and $e_2^{(1)}$ with $e_1^{(1)} = P_{\rm ref} - P_{\rm out}$ and $e_2^{(1)} = \beta_c - \beta$ in this study. The proposed ENN [25], [26], takes the feedback into account, and a better learning efficiency can be obtained. Moreover, to make the neurons sensitive to the history of input data, self-connections of the context nodes and output feedback node are added. So, the proposed ENN combines the ability of dealing with nonlinear problems, can effectively improve the convergence precision and reduce learning time. The signal propagation and the basic function in each layer are introduced as follows.

Layer 1: Input Layer

In the input layer, the node is defined by

$$\text{net}_i^{(1)} = e_i^{(1)}(k) \tag{16}$$

$$x_i^{(1)}(k) = f_i^{(1)}\left(\text{net}_i^{(1)}(k)\right) = \text{net}_i^{(1)} \tag{17}$$

where *k* represents the *k*th iteration, $e_i^{(1)}(k)$ and $x_i^{(1)}(k)$ are the input and the output of the layer, respectively.

Layer 2: Hidden Layer

In the hidden layer, the node is defined by

$$\text{net}_j^{(2)} = \sum_i W_{ij} \times x_i^{(1)}(k) + \sum_r W_{rj} \times x_r^{(3)}(k) \tag{18}$$

$$x_j^{(2)}(k) = \frac{1}{1+\exp(-\text{net}_j^{(2)})} \tag{19}$$

where $x_i^{(1)}$ and $x_r^{(3)}$ are input and $x_j^{(2)}(k)$ is output of the hidden layer. $x_r^{(3)}(k)$ is also the output of the context layer, and W_{ij} and W_{rj} are the connecting weights of input neurons to hidden neurons and context neurons to hidden neurons, respectively.

Layer 3: Context Layer

In the context layer, the node input and output are represented as

$$x_r^{(3)}(k) = \alpha x_r^{(3)}(k-1) + x_j^{(2)}(k-1) \tag{20}$$

where $0 \le \alpha < 1$ is the self-connecting feedback gain.

Layer 4: Output Layer

In the output layer, the node input and output are represented as

$$\text{net}_o^{(4)}(k) = \sum_j W_{jo} \times x_j^{(2)}(k) \tag{21}$$

$$y_o^{(4)}(k) = f_o^{(4)}(\text{net}_o^{(4)}(k)) = \text{net}_o^{(4)}(k) = i_q^* \tag{22}$$

where W_{jo} is the connecting weight of hidden neurons to output neurons, and $y_o^{(4)}(k)$ is the output of the improved ENN and also the control effort of the proposed controller.

Once the ENN has been initialized, a supervised learning is used to train this system based on gradient descent. The derivation is the same as that of the back-propagation algorithm [25], [26]. It is employed to adjust the parameters W_{jo}, W_{rj}, and W_{ij} of the ENN by using the training patterns. By recursive application of the chain rule, the error term for each layer is calculated, and updated. The purpose of supervised learning is to minimize the error function *E* expressed as

$$E = \frac{1}{2}\left(P_{\rm out} - P_{\rm ref}\right)^2 = \frac{1}{2}e^2 \tag{23}$$

where $P_{\rm out}$ and $P_{\rm ref}$ represent the actual output power and the reference output power of the generator, respectively, and e denotes the tracking error. A common supervised training algorithm is used in this paper, the essential features can be seen in [25] and [26].

D. Harmonic Analysis

The harmonic currents pose one big challenge to the measurement of power quality. It requires great accuracy, even for higher frequencies, since the measurement refers to interharmonics that are in the range of 0.1% of the rated current.

Furthermore, the total harmonic distortion (THD) of the voltage, calculated according to (24), has to be less than 8%:

$$\text{THD} = \left[\sum_{h=2}^{40}(u_h)^2\right]^{1/2} \tag{24}$$

where harmonic voltages is u_h, and h denotes the harmonic order.

With regard to high-order harmonics, EN 50160 standard does not specify any limits but states that high-order harmonics are usually small, though fairly unpredictable. The THD was $\text{THD} = 4.61\%$ for nominal phase-to-phase voltage.

TABLE I
SIMULATION PARAMETERS

Wind Induction Generator	
Rated Power (kW)	2
Voltage (V)	220
Frequency (Hz)	60
Inertia	0.7065
No of Pole Pairs	2
Wind speed (m/s)	8~12
Diesel Synchronous Generator	
Rated Power (kW)	12
Voltage (V)	220
Frequency (Hz)	60
Inertia	0.8
No of Pole pair	2
PV Array	
Maximum power of Module Unit (W)	200.143, 25 □, 1000W/m^2
Module Number	4×4=16
Total Power Rating (kW)	0.2×16=3.2
Unit Rated Voltage (V)	26.3
Unit Rated Current (A)	7.61
Irradiance level (W/m^2)	600~1000
Battery Energy Storage System	
Rated Voltage (V)	180
Capacity (kWH)	10
Load	
Capacity (kW)	3~8
Grid	
Voltage (V)	220
Frequency (Hz)	60
Phase	3

V. SIMULATION RESULTS

The hybrid system shown in Fig. 1 is implemented in the MATLAB/Simpower environment. Parameters of the WECS, the diesel generator, and the PV system used in the simulation are shown in Table I. Many tests were conducted to show performance of the model under various conditions, with the comparison of various MPPT schemes [27]–[32] including the typical PI control and P&O method.

A. MPPT System Performance

1) Wind Power MPPT: Time domain simulation was run for the hybrid power system with constant load under sufficient wind and irradiance. The output power from WECS is shown in Fig. 13. From Fig. 13, it can be seen that the ENN controller provides a better control performance than PI with less transient and smaller vibrations. The transient response at the starting point can be seen clearly that PI fluctuates more, while the ENN oscillates only slightly. The average power is 1.88 kW. Compared with that of the PI control, it increases by 6.2%. With different wind speeds, the performance comparison is shown in Table II. More comparisons with other referenced methods are summarized in Table III.

2) Solar Power MPPT: The output power from PV is shown in Fig. 14. From Fig. 14, we can see that the RBFN controller provides a better performance than P&O, both in the transient and the stability. The average power is 2.7 kW. Compared with that of P&O, it increases by 14.89%. The RBFN method can quickly and accurately track the maximum power output for solar array.

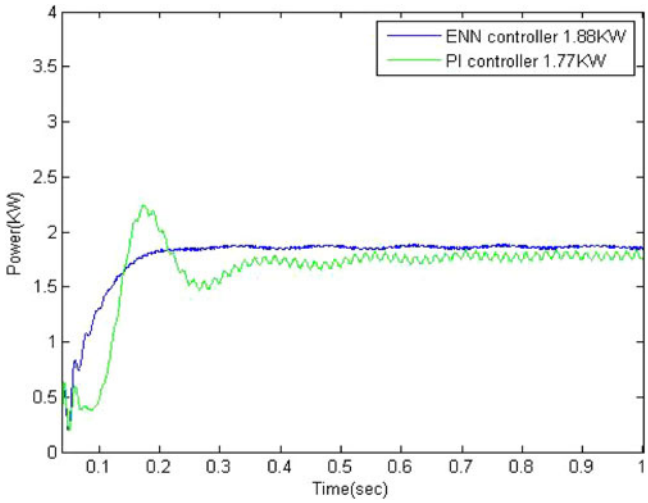

Fig. 13. MPPT tracking response of the WECS.

TABLE II
PERFORMANCE COMPARISON OF THE ENN AND PI CONTROLLER

Controller Type	Wind speed	Power Coefficient (Cp)	Pitch angle (degree)	Average power (kW)
ENN	12*m/s*	0.482	-0.07	1.88
	8*m/s*	0.481	-0.08	0.22
PI	12*m/s*	0.465	-0.55	1.77
	8*m/s*	0.37~0.42	-0.2~-0.55	0.03

TABLE III
PERFORMANCE COMPARISON WITH OTHER REFERENCED METHODS

Algorithm	Power extraction Efficiency (%)	Max. error for optimum C_p (%)	MPPT Accuracy (%)	Transient response (sec)
ENN	85%	0.42%	0.3%	0.3
PI	68%	29.7%	2.5%	0.7
[28]-[30]	80%	23.5%	2.5%	4

B. MPPT PV System Response

Fig. 15(a) and (b) shows the *P–V* and *P–I* of the PV system for MPPT. Voltage and current of responses are shown in Fig. 16(a) and (b), respectively. It shows a robust control performance of the proposed algorithm.

C. MPPT With Load Change

With sufficient wind and irradiance, Figs. 17 and 18 show the comparison of the proposed algorithms with PI and P&O

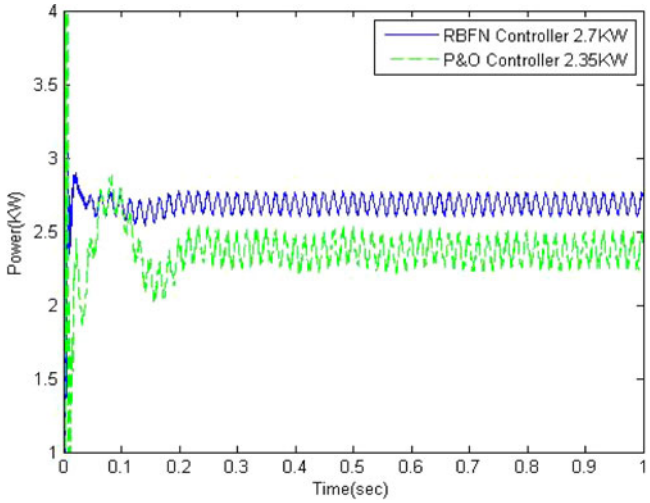

Fig. 14. MPPT tracking response of the PV system.

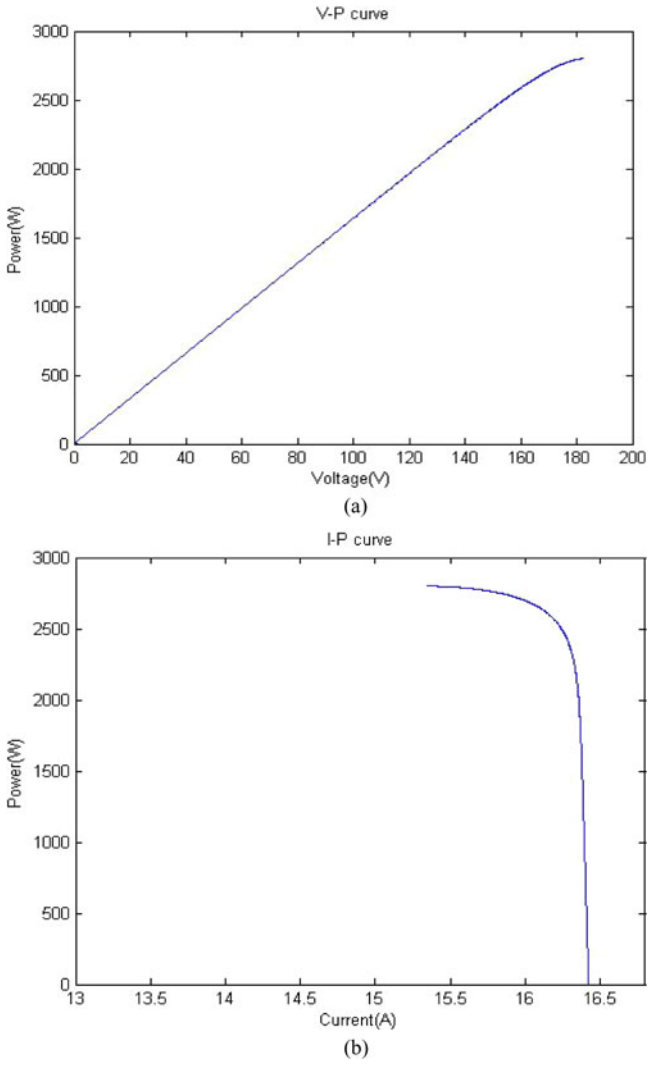

Fig. 15. MPPT responses of the PV generation system. (a) Voltage-power curve. (b) Current-power curve.

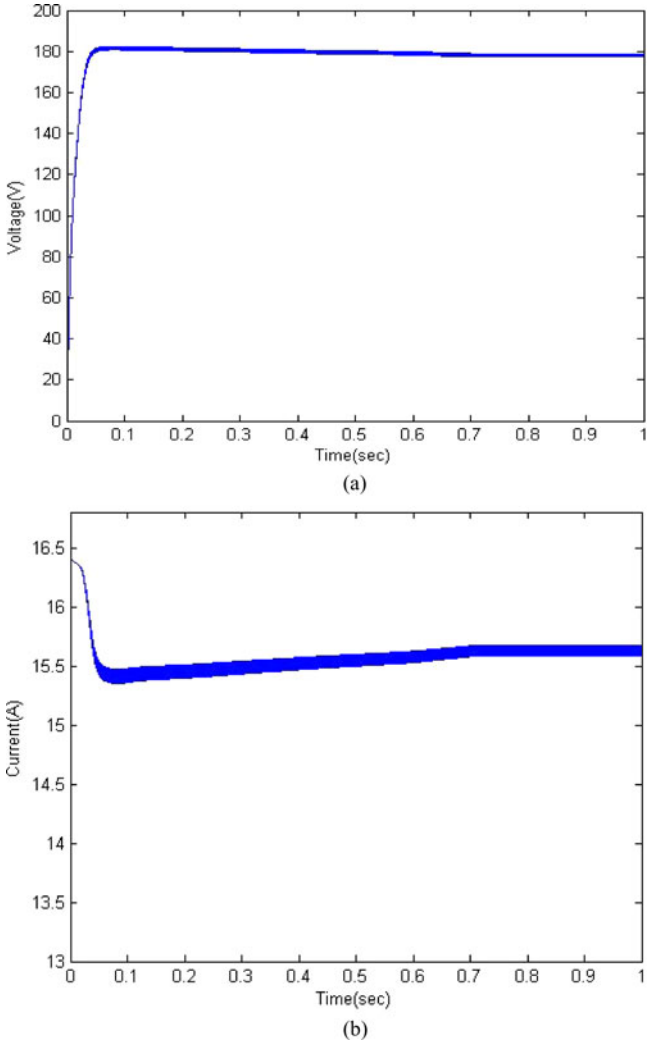

Fig. 16. MPPT voltage and current of the PV system. (a) System voltage. (b) System current.

methods for a sudden load change from 3 to 4 kW. The dc-link voltage slightly decreases and then recovers in around 0.1 s. The grid frequency response will not change as can be seen in Fig. 19. The proposed method can track faster with a more stable output power under load disturbance.

D. MPPT Under Variable Conditions

This case demonstrates a changing environment, where at $t = 5$ s we have

1) the wind speed changed from 12 to 8 m/s;
2) the irradiance level changed from 1000 to 600 W/m^2;
3) and the load changed from 7 to 8 kW.

We can see from Fig. 20 that with the drop of wind speed, the wind power also dropped to a low level around 0.2 kW. The diesel generator works with the wind turbine and PV array to meet the demand by picking up more load. With a short transient in the beginning, the hybrid system quickly reaches a stable operation. From Fig. 3, the relationship between the optimal rotational speed and the power of the DGS is almost

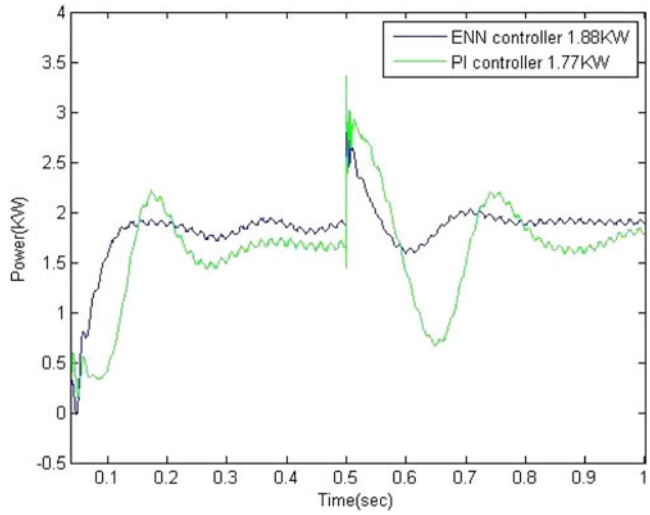

Fig. 17. Wind MPPT tracking under sudden load change.

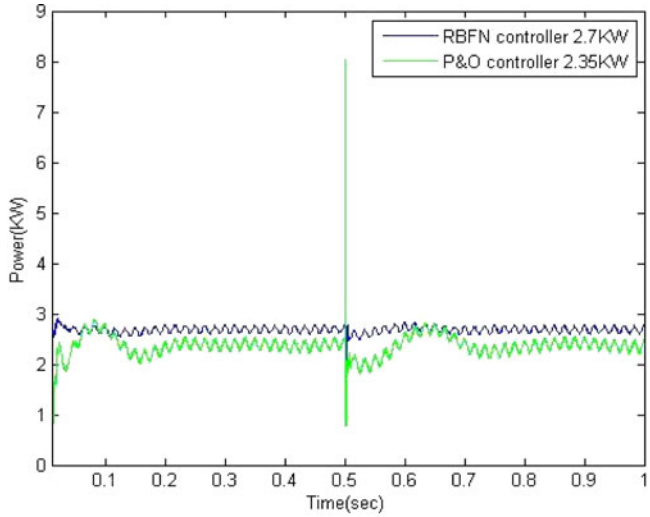

Fig. 18. PV MPPT tracking under sudden load change.

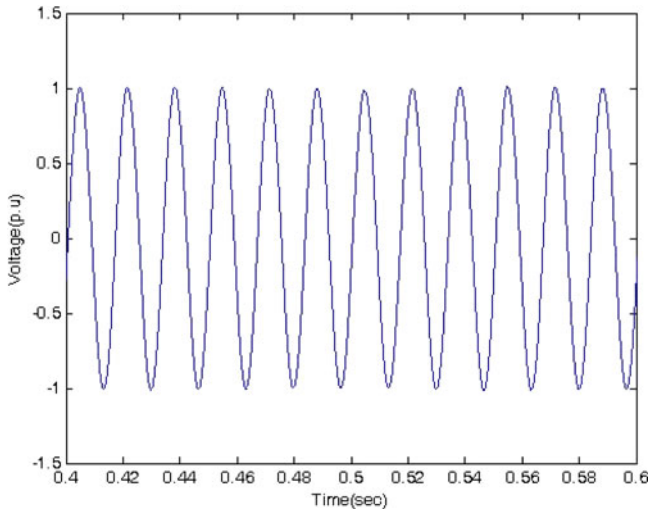

Fig. 19. Grid voltage under sudden load change at $t = 0.5$.

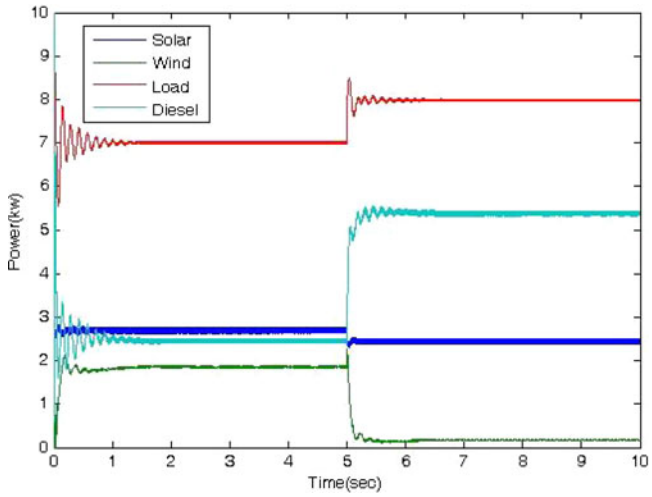

Fig. 20. MPPT tracking under sudden environment change at $t = 5$.

linear in this research. With 7-kW load, the optimal speed of the DGS is 1566 r/min, i.e., 43% rated speed. With 8-kW load, the control strategy drives the generator to a new optimum speed of 1820 r/min, i.e., 51% rated speed. The fuel savings at these reduced speeds are around 19% and 11% in comparison with the rated speed, respectively.

VI. Conclusion

In this paper, a solar and diesel–wind hybrid generation system was proposed and implemented. This stand-alone hybrid generation system can effectively extract the maximum power from the wind and solar energy sources. From the case studies, it shows that voltage and power can be well controlled in the hybrid system under a changing environment. An efficient power sharing technique among energy sources are successfully demonstrated with more efficiency, a better transient and more stability, even under disturbance.

The simulation model of the hybrid system was developed using MATLAB/Simulink. The load frequency is regulated by the diesel generator by imposing the rotor currents with the slip frequency. The electrical torque of the WECS generator is controlled to drive the system to the rotational speed where maximum energy can be captured. Depending on the load size and the power supplied by the WECS generator, the control system regulates the DGS rotational speed to minimize the fuel consumption.

In the future work, the proposed hybrid topology can be tested by using an experimental system with optimal speed tracking algorithms for the diesel engine control, vector control will be used for the wind-driven IG, with the control of the PV generation system implemented in one of the DSP boards. All the proposed control schemes will be implemented by using a real-time workshop, which is online trained by MATLAB/Simulink and implemented by dSPACE. The real-time process can run in a dSPACE that includes a TMS320C32 floating-point DSP. The wind power generation and PV generation of the hybrid

generation system can be independently controlled, hence achieving the MPPT simultaneously.

REFERENCES

[1] G. Abad, M. A. Rodriguez, G. Iwanski, and J. Poza, "Direct power control of doubly-fed-induction-generator-based wind turbine under unbalanced grid voltage," *IEEE Trans. Power Electron.*, vol. 25, no. 2, pp. 442–452, Feb. 2010.

[2] S. M. B. Wilmshurst, "Control strategies for wind turbines," *Wind Eng.*, vol. 12, pp. 236–249, Jul. 1988.

[3] A. J. Rudell, J. A. M. Bleijs, L. Freris, D. G. Infield, and G. A. Smith, "A wind diesel system with variable speed flywheel storage," *Wind Eng.*, vol. 17, pp. 129–145, May 1993.

[4] R. Dettmer, "Revolutionary energy—A wind/diesel generator with flywheel storage," *Inst. Electr. Eng. Rev.*, vol. 36, pp. 149–151, Apr. 1990.

[5] Z. Chen and Y. Hu, "A hybrid generation system using variable speed wind turbines and diesel units," in *Proc. IEEE Ind. Electron. Soc. Annu. Meeting Conf.*, Nov. 2003, pp. 2729–2734.

[6] B. S. Borowy and Z. M. Salameh, "Dynamic response to a stand-alone wind energy conversion system with battery energy storage to a wind gust," *IEEE Trans. Energy Convers.*, vol. 12, no. 1, pp. 73–78, Mar. 1997.

[7] N. Femia, G. Petrone, G. Spagnuolo, and M. Vitelli, "Optimization of perturb and observe maximum power point tracking method," *IEEE Trans. Power Electron.*, vol. 20, no. 4, pp. 963–739, Jul. 2005.

[8] B. Yang, Y. Zhao, and X. He, "Design and analysis of a grid-connected photovoltaic power system," *IEEE Trans. Power Electron.*, vol. 25, no. 4, pp. 992–1000, Apr. 2010.

[9] R. Chedid and S. Rahman, "Unit sizing and control of hybrid wind-solar power systems," *IEEE Trans. Energy Convers.*, vol. 12, no. 1, pp. 79–85, Mar. 1997.

[10] W. D. Kellogg, M. H. Nehrir, G. Venkataramanan, and V. Greez, "Generation unit sizing and cost analysis for stand-alone wind, photovoltaic, and hybrid wind/PV systems," *IEEE Trans. Energy Convers.*, vol. 13, no. 1, pp. 70–75, Mar. 1998.

[11] R. Chedid and S. Rahman, "A decision support technique for the design of hybrid solar–wind power systems," *IEEE Trans. Energy Convers.*, vol. 13, no. 1, pp. 76–83, Mar. 1998.

[12] D. Das, R. Esmaili, L. Xu, and D. Nichols, "An optimal design of a grid connected hybrid wind/photovoltaic/fuel cell system for distributed energy production," in *Proc. 32nd Annu. Conf. IECON*, Nov. 6–10, 2005, pp. 2499–2504.

[13] F. Giraud and Z. M. Salameh, "Steady-state performance of a grid connected rooftop hybrid wind–photovoltaic power system with battery storage," *IEEE Trans. Energy Convers.*, vol. 16, no. 1, pp. 1–7, Mar. 2001.

[14] S. Seshagiri and H. K. Khail, "Output feedback control of nonlinear systems using RBF neural networks," *IEEE Trans. Neural Netw.*, vol. 11, no. 1, pp. 69–79, Jan. 2000.

[15] H. Li, K. L. Shi, and P. G. McLaren, "Neural-network-based sensorless maximum wind energy capture with compensated power coefficient," *IEEE Trans. Ind. Appl.*, vol. 41, no. 6, pp. 548–1556, Nov./Dec. 2005.

[16] E. Muljadi and C. P. Butterfield, "Pitch-controlled variable-speed wind turbine generation," *IEEE Trans. Ind. Appl.*, vol. 37, no. 1, pp. 240–246, Jan./Feb. 2001.

[17] J. L. Elman, "Finding structure in time," *Cognitive Sci.*, vol. 14, no. 2, pp. 179–211, 1990.

[18] Y. M. Cheng, Y. C. Liu, S. C. Hung, and C. S. Cheng, "Multi-input inverter for grid-connected hybrid PV/wind power system," *IEEE Trans. Power Electron.*, vol. 22, no. 3, pp. 1070–1076, May 2007.

[19] J. M. Kwon, B. H. Kwon, and K. H. Nam, "Three-phase phtotvoltaic system with three-level boosting MPPT control," *IEEE Trans. Power Electron.*, vol. 23, no. 5, pp. 2319–2327, May 2008.

[20] M. Veerachary, T. Senjyu, and K. Uezato, "Voltage-based maximum power point tracking control of PV system," *IEEE Trans. Aerosp. Electron. Syst.*, vol. 38, no. 1, pp. 262–270, Jan. 2002.

[21] *IEEE Recommended Practice for Excitation System Models for Power System Stability Studies, IEEE Power Engineering Society,* IEEE Std 421.5TM-2005, Apr. 2006.

[22] S. Liu and R. A. Dougal, "Dynamic multiphysics model for solar array," *IEEE Trans. Power Electron.*, vol. 17, no. 2, pp. 285–294, Jun. 2002.

[23] C. T. Lin and C. S. George Lee, *Neural Fuzzy Systems*: Prentice-Hall, Inc., 1996.

[24] S. Wan, H. Li, and Y. Li, "Adaptive radial basis function network and its application in turbine-generator vibration fault diagnosis," in *Proc. Power Syst. Technol. Conf.*, 2002, vol. 3, pp. 1607–1610.

[25] H. Liu, S. Wang, and P. Ouyang, "Fault diagnosis based on improved Elman neural network for a hydraulic servo system," in *Proc. Int. Conf. Robot., Autom. Mechatronics*, Dec. 2006, pp. 1–6.

[26] F. J. Lin and Y. C. Hung, "FPGA based Elman neural network control system for linear ultrasonic motor," *IEEE Trans. Ferr. Ultras. And Freq. Control.*, vol. 56, no. 1, pp. 101–113, Jan. 2009.

[27] J. T. Bialasiewicz, E. Muljadi, and R. G. Nix, "Simulation-based analysis of dynamics and control of autonomous wind–diesel hybrid power systems," *Int. J. Power Energy Syst.*, vol. 22, no. 1, pp. 24–33, 2002.

[28] S. Morimoto, H. Nakayama, M. Sanada, and Y. Takeda, "Sensorless output maximization control for variable-speed wind generation system using IPMSG," *IEEE Trans. Ind. Appl.*, vol. 41, no. 1, pp. 60–67, 2005.

[29] Q. Wang and L. Chang, "An intelligent maximum power extraction algorithm for inverter-based variable speed wind turbine systems," *IEEE Trans. Energy Convers.*, vol. 19, no. 5, pp. 1242–1249, Sep. 2004.

[30] R. Cardenas, R. Pena, J. Proboste, G. Asher, and J. Clare, "MRAS observer for sensorless control of standalone doubly fed induction generators," *IEEE Trans. Energy Convers.*, vol. 20, no. 4, pp. 710–718, Dec. 2005.

[31] A. Payman, S. Pierfederici, and F. Meibody-Tabar, "Energy management in a fuel cell/supercapacitor multisource/multiload electrical hybrid system," *IEEE Trans. Power Electron.*, vol. 24, no. 12, pp. 2681–2691, Dec. 2009.

[32] S. L. Brunton, C. W. Rowley, S. R. Kulkarni, and C. Clarkson, "Maximum power point tracking for photovoltaic optimization using ripple-based extremum seeking control," *IEEE Trans. Power Electron.*, vol. 25, no. 10, pp. 2531–2540, Oct. 2010.

Whei-Min Lin (M'87) was born in 1954. He received the B.S.E.E. degree from the National Chao-Tung University, Hsin-Chu, Taiwan, and the M.S.E.E. degree from the University of Connecticut, Storrs, and the Ph.D. E.E. degree from the University of Texas, Arlington, in 1985.

He was with Chung-Hwa Institute for Economic Research, Taiwan, as a Visiting Rresearcher after his graduation. He joined Control Data Crop. in 1986, Minneapolis, MN, and was with Control Data Asia in 1989. He has been with National Sun Yat-Sen University, Kaohsiung, Taiwan, since 1991. His research interests are GIS, Distribution System, SCADA, and Automatic Control System.

Dr. Lin is a member of IEEE and Tau Beta Pi.

Chih-Ming Hong was born in 1972. He received the B.S.E.E. degree from the Kaohsiung Polytechnic Institute, Kaohsiung, Taiwan, in 1997 and the M.S.E.E. degree from the Chung Yuan Christian University, Chung Li, Taiwan, in 1999. He is currently working toward the Ph.D. degree at National Sun Yat-Sen University, Kaohsiung, Taiwan.

His research interests include motor drive systems, DSP, power electronics, control theory applications, and renewable energy systems.

Chiung-Hsing Chen was born in 1961. He received the B.S. degree in electrical engineering from the Feng Chia University, Taichung, Taiwan, in 1983 and the M.S. and Ph.D. degrees in electrical and computer engineering from the Ohio University, Athens, in 1994.

He is currently with National Kaohsiung Marine University, Kaohsiung, Taiwan, where he has been since 1994. His main interests include DSP, SCADA, and intelligent control.